Theoretical study of the C–F bond activation in methyl fluoride by alkaline-earth metal monocations

ARTICLE *in* THEORETICAL CHEMISTRY ACCOUNTS · FEBRUARY 2011

Impact Factor: 2.23 · DOI: 10.1007/s00214-010-0864-x

Theor Chem Acc (2011) 128:609–618
DOI 10.1007/s00214-010-0864-x

REGULAR ARTICLE

Theoretical study of the C–F bond activation in methyl fluoride by alkaline-earth metal monocations

Adrián Varela-Álvarez · José Ángel Sordo · Pilar Redondo · Antonio Largo · Carmen Barrientos · Víctor M. Rayón

Received: 26 June 2010 / Accepted: 25 November 2010 / Published online: 8 December 2010

Abstract Reactions of methyl fluoride with bare alkaline-earth metal monocations (Mg^+, Ca^+, Sr^+, and Ba^+) were studied using theoretical methods. Thermochemical data were calculated using density functional theory in conjunction with polarized 3-ζ and 4-ζ basis sets. Variational/conventional microcanonical transition state theory was used for the calculation of the reaction rate constants over a large range of temperatures. According to our calculations, the Ca^+, Sr^+, and Ba^+ reactions with CH_3F proceed to yield CaF^+, SrF^+, and BaF^+, in agreement with the experimental observation. The theoretically predicted global rate constants are in reasonable agreement with the experimental data. In the case of Mg^+, the large value of the computed energy barrier associated with the "inner" transition structure is fully consistent with the limited progress experimentally observed for this reaction. The importance of bottlenecks other than the "inner" transition state is highlighted and its mechanistic implications discussed. Particularly, our calculations suggest that the studied processes proceed through a "harpoon-like" mechanism.

Published as part of the special issue celebrating theoretical and computational chemistry in Spain.

A. Varela-Álvarez · J. Á. Sordo
Departamento de Química Física y Analítica,
Laboratorio de Química Computacional, Facultad de Química,
Universidad de Oviedo, Julián Clavería 8, 33006 Oviedo,
Principado de Asturias, Spain

P. Redondo · A. Largo · C. Barrientos · V. M. Rayón (✉)
Departamento de Química Física y Química Inorgánica,
Facultad de Ciencias, Universidad de Valladolid,
47005 Valladolid, Spain
e-mail: victormanuel.rayon@uva.es

Keywords C–F bond activation · Mechanism · Kinetics · Microcanonical transition state theory

Abbreviations

BDE	Bond dissociation energy
DFT	Density functional theory
ICP/SIFT	Inductively coupled plasma/selected-ion flow tube
SET	Single-electron transfer
DCP	Distinguished coordinate path
μVTST	Microcanonical variational transition state theory
MPA	Mulliken Population Analysis
SIE	Second ionization energy

1 Introduction

Activation of carbon–fluorine bonds constitutes a very important field in contemporary chemistry (see [1] and references therein). Due to its strong bond dissociation energy (BDE), the largest among the carbon single bonds, selective functionalization of C–F bonds is anything but an easy task. Although of larger practical relevance in synthetic chemistry, C–F activation reactions have also been the subject of many systematic gas-phase experiments aiming to investigate intrinsic properties of these processes [1]. Very recently, Zhao et al. investigated the reaction of fluoromethane with 46 different atomic cations in the gas phase using an inductively coupled plasma/selected-ion flow tube (ICP/SIFT) tandem mass spectrometer [2]. Taking into account the wide variety of atomic cations that have been studied (from

the fourth-, fifth-, and sixth-periods, from K^+ to Po^+), the rich chemistry observed in these reactions cannot be a surprise. More than half of the reactions (26 out of 46) proceeded by addition to yield the $[MCH_3F]^+$ adduct whereas 13 exhibited fluorine atom transfer to produce MF^+ and CH_3. Among the remaining 7 reactions, 2 did not show products in the flow regime investigated and 5 proceeded by either HF elimination (As^+) or dehydrogenation (W^+, Os^+, Ir^+, and Pt^+). Besides, Zhao et al. [2] have observed many interesting periodic trends in the global rate coefficients for these reactions which certainly deserve further analysis. The gas-phase reactivity of fluoromethane with lanthanide monocations (Ce^+, Pr^+, Sm^+, Ho^+, Tm^+, and Yb^+) has also been examined by Fourier-transform ion cyclotron resonance mass spectrometry [3]. From that study, Cornehl et al. suggested a single-electron transfer (SET) or 'harpoon' mechanism for the F atom abstraction process that would then proceed by the transfer of one electron from the lanthanide monocation to the fluorine atom in the encounter adduct Ln^+FCH_3, followed by fluorine anion transfer from the CH_3 radical to yield the final LnF^+ product. Cornehl et al. have argued that this mechanism is supported by the correlation they have found between the reactivity of the lanthanide monocations and their second ionization energy (SIE). The reaction of fluoromethane and Ca^+ to yield CaF^+ has also been the subject of a joint experimental and theoretical study by Harvey et al. [4]. For this reaction, the authors reported that calcium is about 4 times more reactive than lanthanide monocations with a similar SIE. This clearly suggests that the F atom transfer mechanism is not fully understood yet and that some other factors involved in these reactions have to be taken into account.

In a very recent paper [5], we have theoretically investigated the reaction between calcium monocation and CH_3F. On the one hand, we carried out high-level electronic structure calculations in order to characterize the potential energy surface (PES) of this reaction as well as to provide reliable thermochemical information. Our electronic structure calculations basically support the theoretical study of Harvey et al. carried out several years ago except for one important point: in contrast with their conclusion that DFT is unable to model this reaction, we have shown that the use of appropriate recent density functionals, particularly those developed specifically for kinetics, correctly describes the energetics of these processes.

We additionally carried out kinetics calculations in the framework of statistical theories (energy and total angular momentum resolved microcanonical transition state theory). The theoretically predicted thermal rate constant for this reaction at 295 K (7.8×10^{-11}–2.5×10^{-9} cm^3 $molecule^{-1}$ s^{-1})[1] agrees reasonably well with the experimental value obtained by Zhao et al. [$(2.6 \pm 0.8) \times 10^{-10}$ cm^3 $molecule^{-1}$ s^{-1}]. This range of rate constants covers the whole set of density functionals and basis sets used in our previous study on the Ca^+ reaction. The lower and upper values of the range were obtained at the B3LYP/TZVPP and MPW1K/TZVPP levels of theory, respectively. Besides, we have also shown that a two transition state model (with explicit consideration of an 'outer' transition state in the entrance channel) is mandatory to correctly model the kinetics of this reaction.

The gas-phase kinetics study of Zhao et al. [2] also provides results for the reaction of Sr^+ and Ba^+ with fluoromethane which also proceed via F atom transfer to yield SrF^+ and BaF^+ as a main primary product. This reaction is clearly slower with Sr^+ [$(k = (1.4 \pm 0.4) \times 10^{-11}$ cm^3 $molecule^{-1}$ s^{-1}] and Ba^+ [$(6.4 \pm 1.9) \times 10^{-11}$] than with Ca^+ [$(2.6 \pm 0.8) \times 10^{-10}$]. On the other hand, no experimental kinetics studies have been carried out, to the best of our knowledge, for the reaction of CH_3F with magnesium monocation. However, the fact that reactions of Mg^+ with saturated hydrocarbons [6] and small inorganic ligands like NH_3, CO, and O_2. [7, 8] either do not show products or proceed by molecular addition suggests that methyl fluoride reaction with Mg^+ might involve a different mechanism than with Ca^+ and Sr^+. We also point out that Mg^+–CH_3F 1:1 clusters have been indeed isolated in preparation for photodissociation experiments [9–11], thus suggesting that this complex should be relatively stable toward dissociation back to reactants.

In this article, we have carried out theoretical studies on the thermochemistry and kinetics of the reactions between Mg^+, Ca^+, Sr^+ and Ba^+ with CH_3F. To our knowledge, no previous theoretical calculations have been performed for these systems before (except for the characterization of the encounter complex Mg^+CH_3F in Refs. [9–11] and the already mentioned results for the Ca^+ reaction by Harvey et al. [4] and our own previously published calculations [5]).

2 Methods

2.1 Electronic structure calculations

Density functional theory (DFT) has been used to fully explore the four potential energy surfaces (PES). Based on our previous experience on the Ca^+ reaction [5], we

[1] The rate constants reported in Ref. [5] are slightly different from those presented here as a consequence of a correction in the number of rotational levels considered in the calculations. The modification does not affect our previous conclusions at all.

Scheme 1 Schematic representation of the potential energy surface for the reaction between $M^+(^2S)$ with CH_3F (M=Mg, Ca, Sr, Ba)

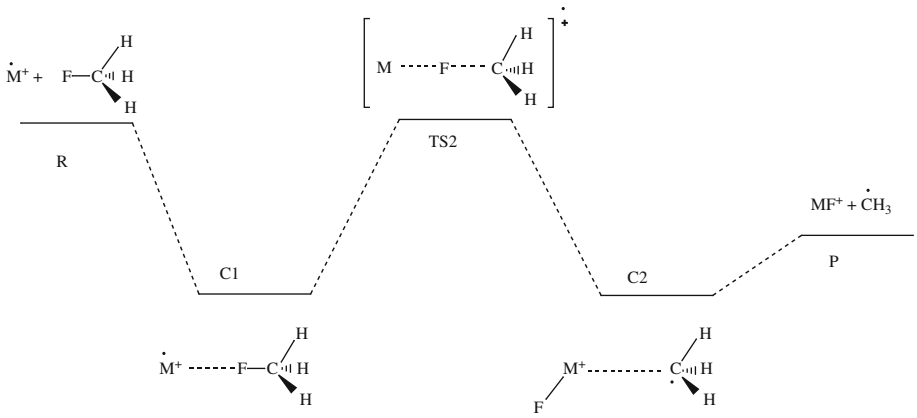

have selected for this study the modified Perdew–Wang-1-parameter functional (MPW1K) [12] that has been developed specifically for kinetics. In conjunction with this functional, we have used 3-ζ and 4-ζ basis sets from three different laboratories, namely Ahlrichs' (TZVPP and QZVPP) [13], Dunning's (cc-pVTZ and cc-pVQZ)[2] [14–16] and Jensen's (pc-2 and pc-3) [17, 18]. Most of these basis sets have been obtained from the basis set exchange [19, 20]. Ahlrichs' basis sets for Sr and Ba include a small-core effective core potential (ECP); thus, 9 electrons are treated explicitly. For the rest of elements, all bases employed are all-electron basis sets. Stationary points on the PES have been characterized by checking the negative eigenvalues of the analytical Hessian (zero for local minima and one for first-order saddle points corresponding to transition structures). Reaction paths have been checked by performing intrinsic reaction coordinate (IRC) calculations [21, 22]. Both the zero-point energy and thermal contributions to enthalpy (ΔH), entropy (ΔS), and Gibbs free energy (ΔG) have been estimated within the ideal gas, rigid rotor, and harmonic oscillator approximations [23]. A temperature of 298.15 K and a pressure of 1 atm have been considered. All the electronic structure and statistical thermodynamics calculations were performed with the GAUSSIAN 03 package of programs [24].

2.2 Kinetics calculations

We refer the reader to our previous study on the reaction between Ca^+ and CH_3F [5] for a detailed description of the kinetics model we have used. Here, we summarize the most important features of that model that is based on previous ideas by Mozurkewich and Benson [25] who developed some time ago a kinetics formulation within the context of the Rice-Ramsperger-Kassel-Marcus (RRMK) theory for processes with an energy profile similar to that schematically represented in Scheme 1. The most important feature of this profile is the appearance of two wells, the first of which is reached steadily from reactants without surmounting an electronic potential barrier. For the kinetics calculations concerning the formation of both the initial intermediate and the exit channel (where no saddle point was located on the PES), we have thus adopted the *E*, *J*-resolved microcanonical variational transition state theory (μVTST) in its vibrator formulation [26, 27]. More specifically, a distinguished-coordinate path (DCP) [28, 29] was constructed for each channel, and subsequently, projected frequencies were obtained for each point on the path. The sum of states, $W(E, J)$, at energy lower than E and angular momentum J has been computed by means of the Forst algorithm [30]. Under steady-state conditions, the global rate constant can be expressed:

$$k_{\text{global}} = \frac{\left(\frac{2\pi\mu k_B T}{h^2}\right)^{-3/2}}{hQ_R} \sum_{J=0}^{\infty} \int_{V_{\max}}^{\infty} \mathrm{d}E\, W_1(E,J) \times \frac{W_2(E,J)\cdot W_3(E,J)}{W_2(E,J)\cdot W_3(E,J) + W_1(E,J)\left[W_2(E,J)+W_3(E,J)\right]} e^{-E/RT} \quad (1)$$

where $V_{\max}$ is the largest value from among the energy barriers associated with the energy profile (see Scheme 1), Q_R represents the product of the partition functions of reactants, where the center of mass motion partition function has been factored out, and W_1, W_2, and W_3 represent the sum of the states at the entrance channel, the **TS2** transition state, and the exit channel, respectively. Besides, T is the temperature; R, k_B, and h are gas, Boltzmann and Planck constants, and μ is the reduced mass. Reaction symmetry factors have been included in the sums of states, $W_i(E, J)$. Our own routines were employed to carry out the kinetics calculations [5].

[2] The correlation consistent basis set for Mg has been obtained from the Basis Set Exchange (BSE) (see Refs. [19, 20]). This basis set has not been published until recently (Ref [16]) and has been slightly modified with respect to the preliminary version stored in the BSE.

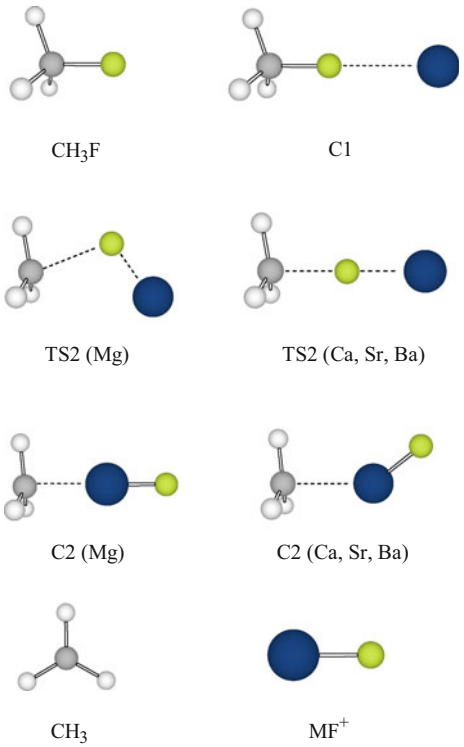

Fig. 1 Structures located on the PES for the reaction between $M^+(^2S)$ with CH_3F (M=Mg, Ca, Sr, Ba). Geometrical parameters are collected in Table 1

Table 1 Geometrical parameters (angstroms and degree) for the different species involved in the reaction $M^+(^2S) + CH_3F$ (M=Mg, Ca, Sr, Ba) at the MPW1K/TZVPP level of theory

		CH_3F	**C1**	**TS2**	**C2**	MF^+
$[MgCH_3F]^+$	C–F	1.365	1.445	2.095		
	C–Mg			2.763	2.240	
	Mg–F		1.975	1.750	1.697	1.688
	Mg–F–C		180.0	91.4	0.0	
	H–C–Mg–F				–	
$[CaCH_3F]^+$	C–F		1.430	1.950		
	C–Ca				2.737	
	Ca–F		2.235	2.010	1.885	1.869
	Ca–F–C		180.0	180.0	101.8	
	H–C–Ca–F				0.0	
$[SrCH_3F]^+$	C–F		1.423	1.920		
	C–Sr				2.919	
	Sr–F		2.410	2.148	2.001	1.986
	Sr–F–C		180.0	180.0	91.4	
	H–C–Sr–F				0.0	
$[BaCH_3F]^+$	C–F		1.417	1.840		
	C–Ba				3.140	
	Ba–F		2.576	2.309	2.111	2.097
	Ba–F–C		180.0	176.0	84.8	
	H–C–Ba–F				0.0	

3 Results

3.1 Thermochemical results

Figure 1 shows the structures located on the PES for the four studied reactions. Values for the most important geometrical parameters are collected in Table 1, whereas Table 2 shows the adiabatic potential energies ($\Delta U_0 = \Delta U$ + zero-point energy) and Gibbs free energies (ΔG) as obtained with three different 3-ζ and 4-ζ basis sets. The MPW1K/TZVPP values for Ca^+ have been already presented in our previous work [5] and are shown here for comparison purposes. As commented above, activation of C–F bonds by alkaline-earth monocations begins with the formation of an encounter complex **C1** in which the metal interacts with fluorine. For the four monocations, this complex has C_{3v} symmetry and an expected $^2A_1$ electronic ground state. The $M^+\cdots FCH_3$ bond distance ranges from 1.975 Å to 2.576 Å and increases, as expected, from Mg^+ to Ba^+. Upon interaction, the C–F distance enlarges 0.080 Å (Mg^+), 0.065 Å (Ca^+), 0.058 Å (Sr^+), and 0.052 Å (Ba^+) with respect to that found in isolated CH_3F. This trend correlates with the bond dissociation energies for **C1** which decrease again downwards in the group (see Table 2; MPW1K/QZVPP values): +25.7 kcal/mol (Mg^+), +22.8 kcal/mol (Ca^+), +19.1 kcal/mol (Sr^+), and +18.5 kcal/mol (Ba^+). As expected, the interaction potential between the metal monocation and CH_3F (whose leading term is the charge–dipole interaction) is attractive for the whole range of $M^+\cdots F$ distances. Thus, no transition structure has been located on the PES for the formation of **C1**. However, as commented in the introduction and discussed in our previous article [5], it is expected that an entropic bottleneck ("outer" transition state **TS1**) appears in this region of the PES.

From **C1**, reaction proceeds through transition structure **TS2** whose structure is depicted in Fig. 1. For Ca^+ and Sr^+, this transition structure has again C_{3v} symmetry (and $^2A_1$ electronic state). In the case of Ba^+, the geometry is slightly distorted with a M^+–F–C angle of 176 degrees. For Mg^+, on the contrary, the M^+–F–C angle notably reduces to 91.4 degrees (see Table 2). Notice, however, that Mg^+–C bond distance is quite large (2.763 Å), which suggests that Mg^+ interacts solely with F in **TS2**, as it was also the case for Ca^+, Sr^+, and Ba^+. As a matter of fact, we have analyzed the topology of the MPW1K/TZVPP electronic charge density for Mg^+ **TS2** and found the expected bond critical points for the interactions $Mg^+\cdots F$ and $F\cdots C$ but no critical point between Mg^+ and C. The M^+–F distance in **TS2** is just 0.062 Å (Mg^+), 0.141 Å (Ca^+), 0.162 Å (Sr^+), and 0.212 Å (Ba^+) longer that this distance in isolated MF^+, suggesting a late transition state for this process. For

Table 2 MPW1K relative energies (kcal/mol) including the zero-point energy (ΔU_0) and relative Gibbs free energies (ΔG; in brackets) as computed at 298 K and 1 atm for the different species involved in the reaction $M^+(^2S) + CH_3F$ (M=Mg, Ca, Sr, Ba) in conjunction with Ahlrichs', Dunning's, and Jensen's 3-ζ and 4-ζ basis sets

	TZVPP		QZVPP		cc-pVTZ		cc-pVQZ		pc-2		pc-3	
$Mg^+ + CH_3F$	0.0	[0.0]	0.0	[0.0]	0.0	[0.0]	0.0	[0.0]	0.0	[0.0]	0.0	[0.0]
C1	−25.3	[−19.6]	−25.7	[−20.0]	−26.6	[−20.8]	−26.3	[−20.5]	−24.8	[−19.0]	−25.7	[−20.0]
TS2	11.1	[15.9]	9.0	[13.6]	9.6	[14.4]	9.1	[13.5]	12.4	[17.3]	9.2	[14.0]
C2	−15.4	[−10.2]	−18.1	[−13.1]	−16.6	[−11.7]	−17.7	[−12.7]	−13.6	[−9.0]	−17.9	[−12.9]
$MgF^+ + CH_3$	13.2	[11.7]	9.9	[8.4]	12.1	[10.6]	10.8	[9.3]	14.5	[13.0]	10.1	[8.6]
$Ca^+ + CH_3F$	0.0	[0.0]	0.0	[0.0]	0.0	[0.0]	0.0	[0.0]				
C1	−21.9	[−16.0]	−22.8	[−17.0]	−23.7	[17.8]	−23.2	[−17.3]				
TS2	−1.1	[4.6]	−3.0	[2.5]	−3.3	[2.3]	−3.4	[2.1]				
C2	−36.9	[−33.0]	−41.9	[−37.4]	−40.6	[−36.0]	−42.3	[−37.7]				
$CaF^+ + CH_3$	−24.3	[−25.9]	−29.1	[−30.7]	−27.7	[−29.3]	−29.3	[−30.9]				
$Sr^+ + CH_3F$	0.0	[0.0]	0.0	[0.0]								
C1	−18.8	[−12.9]	−19.1	[−13.3]								
TS2	2.6	[8.2]	1.3	[6.9]								
C2	−33.6	[−29.7]	−36.9	[−33.1]								
$SrF^+ + CH_3$	−23.6	[−25.3]	−26.5	[−28.2]								
$Ba^+ + CH_3F$	0.0	[0.0]	0.0	[0.0]								
C1	−18.1	[−12.3]	−18.5	[−12.8]								
TS2	1.8	[6.8]	0.4	[4.3]								
C2	−42.1	[−38.5]	−46.1	[−42.5]								
$BaF^+ + CH_3$	−33.9	[−36.4]	−38.3	[−40.0]								

Mg^+, in particular, the C–F bond in **TS2** seems to be almost completely cleaved (C–F = 2.095 Å). Since the carbon–fluorine bond is very strong (113 ± 1 kcal/mol [31]; the MPW1K/QZVPP value is 109.8 kcal/mol), this observation could explain the higher energetic position of Mg^+ **TS2** with respect to reactants (+9.1 kcal/mol) compared to Ca^+ (−3.0 kcal/mol), Sr^+ (+1.3 kcal/mol), and Ba^+ (+0.4 kcal/mol, see Table 2).

Transition structure **TS2** yields a second intermediate, **C2** (see Scheme 1), in which the reaction products, MF^+ and methyl radical, form an addition complex. For Ca^+, Sr^+, and Ba^+, this complex has C_s symmetry (see Fig. 1; Table 1). This means that a branching point should exist along the Ca^+ and Sr^+ reaction path from **TS2** to **C2** that displaces MF^+ out from the C_3 axis. Notice that intermediate **C2** is clearly lower in energy than **C1** (by almost 20 kcal/mol) due to the high fluorine affinity of Ca^+, Sr^+, and Ba^+ which yields very strong M^+–F bonds. On the other hand, intermediate **C2** is also located on the $[MgCH_3F]^+$ PES, but in this case, this structure has C_{3v} symmetry. For Mg^+, **C2** is higher in energy than **C1** due to the low fluorine affinity of Mg^+ (91.9 kcal/mol at the MPW1K/QZVPP level of theory).

Finally, the products of the reaction (MF^+ and CH_3) are formed from **C2** without passing through any electronic potential barrier. Nevertheless, it is again expected that an entropic bottleneck appears in this region of the PES.

Table 2 shows that production of CaF^+, SrF^+, and BaF^+ is clearly exothermic, whereas formation of MgF^+ is endothermic by ca. 10 kcal/mol. This fact again is to be related to the smaller fluorine affinity of Mg^+ (91.9 kcal/mol) with respect to Ca^+ (130.8), Sr^+ (128.0), and Ba^+ (139.7). We point out in passing that our predicted fluorine atom affinities for Ca^+ and Sr^+ are in good agreement with previous experimental [32] (Ca^+: 133.2 ± 2 kcal/mol) and theoretical [33] values (Ca^+: 131.0; Sr^+: 131.7).

We comment now on the performance of different basis sets (Ahlrichs', Dunning's, and Jensen's) in the computation of relative energies (see Table 2). For $[MgCH_3F]^+$, where the three basis sets are available, it is readily seen that the three 4-ζ basis set agree within less than 1 kcal/mol. The corresponding 3-ζ values deviate up to 4.4 kcal/mol from the 4-ζ results. The smaller deviations are found for the cc-pVXZ basis and the largest for pc-n with Ahlrichs' showing intermediate differences. Similar conclusions can be obtained for the Ca monocation for which only Ahlrichs' and Dunning's sets are available: 4-ζ values differ in less than 0.5 kcal/mol and a smaller deviation is found for Dunning's set when comparing 3-ζ and 4-ζ values. Thus, we can conclude that all 4-ζ basis perform

equally well and that Dunning's correlation consistent basis set is an appropriate basis for the study of this kind of reactions. This seems to contrast with conclusions from Boese et al. [34] who have suggested that Dunning's basis were not the most appropriate set to be used in conjunction with density functionals. Let us finally point out that for Ahlrichs' and Jensen's basis set, the relative energy of **TS2** with a 3-ζ basis set still differs in ca. 2 kcal/mol with respect to the 4-ζ values (the range is 1.3–3.2 kcal/mol depending on the metal monocation and the basis set). Notice that if this transition state exercised the full control of the kinetics of these reactions (a point that will be addressed below), such a relative large energy difference should lead to errors of ca. 2 orders of magnitude for the rate constant. Similar differences between the 3-ζ and 4-ζ values are also found for the products of these reactions, MF^+ and CH_3, whose relative stability with respect to reactants seems still not well converged with a 3-ζ basis set.

We have additionally collected in Table 2 the relative Gibbs free energies for the different structures located on the PES. As expected, both transition structures and intermediates are destabilized with respect to reactants because of entropic effects. On the other hand, the products of the reaction, MF^+ and CH_3, are slightly stabilized for the same reason.

3.2 Analysis of the kinetics results

Table 3 collects the global thermal rate constants for the four reactions computed over a wide range of temperatures (135–1,095 K). Taking into account the results commented in the previous section, we have decided to perform the kinetics analysis on the MPW1K/TZVPP PES but

Table 3 Kinetic rate constants (see the text for definitions), in cm^3 $molecule^{-1}$ s^{-1} for the reactions $M^+ + CH_3F$ (M=Mg, Ca, Sr, Ba)

T (K)	Mg^+				Ca^+		
	k_{outer}	k_{inner}	k_{exit}	k_{global}	k_{outer}	k_{inner}	k_{global}
135	3.14×10^{-09}	3.74×10^{-26}	6.81×10^{-30}	4.26×10^{-30}	3.56×10^{-09}	4.04×10^{-09}	7.11×10^{-10}
215	2.52×10^{-09}	1.60×10^{-20}	6.32×10^{-22}	2.64×10^{-22}	3.07×10^{-09}	2.11×10^{-09}	5.59×10^{-10}
295	2.28×10^{-09}	7.48×10^{-18}	3.39×10^{-18}	1.02×10^{-18}	2.84×10^{-09}	1.52×10^{-09}	4.99×10^{-10}
375	2.17×10^{-09}	2.95×10^{-16}	5.17×10^{-16}	1.20×10^{-16}	2.72×10^{-09}	1.29×10^{-09}	4.80×10^{-10}
455	2.10×10^{-09}	3.54×10^{-15}	1.43×10^{-14}	2.69×10^{-15}	2.66×10^{-09}	1.20×10^{-09}	4.80×10^{-10}
535	2.06×10^{-09}	2.18×10^{-14}	1.51×10^{-13}	2.40×10^{-14}	2.62×10^{-09}	1.18×10^{-09}	4.91×10^{-10}
615	2.03×10^{-09}	8.80×10^{-14}	8.84×10^{-13}	1.22×10^{-13}	2.59×10^{-09}	1.21×10^{-09}	5.09×10^{-10}
695	2.00×10^{-09}	2.68×10^{-13}	3.47×10^{-12}	4.27×10^{-13}	2.56×10^{-09}	1.26×10^{-09}	5.33×10^{-10}
775	1.97×10^{-09}	6.67×10^{-13}	1.03×10^{-11}	1.58×10^{-12}	2.54×10^{-09}	1.33×10^{-09}	5.60×10^{-10}
855	1.95×10^{-09}	1.43×10^{-12}	2.50×10^{-11}	2.60×10^{-12}	2.53×10^{-09}	1.42×10^{-09}	5.90×10^{-10}
935	1.93×10^{-09}	2.73×10^{-12}	5.18×10^{-11}	5.09×10^{-12}	2.51×10^{-09}	1.52×10^{-09}	6.23×10^{-10}
1,015	1.92×10^{-09}	4.75×10^{-12}	9.53×10^{-11}	8.92×10^{-12}	2.50×10^{-09}	1.63×10^{-09}	6.57×10^{-10}
1,095	1.91×10^{-09}	7.63×10^{-12}	1.59×10^{-10}	1.43×10^{-11}	2.50×10^{-09}	1.74×10^{-09}	6.92×10^{-10}

T (K)	Sr^+			Ba^+		
	k_{outer}	k_{inner}	k_{global}	k_{outer}	k_{inner}	k_{global}
135	1.60×10^{-08}	4.66×10^{-14}	4.64×10^{-14}	8.77×10^{-09}	6.14×10^{-12}	5.55×10^{-12}
215	9.18×10^{-09}	5.22×10^{-13}	5.17×10^{-13}	5.27×10^{-09}	2.42×10^{-11}	1.99×10^{-11}
295	6.91×10^{-09}	2.05×10^{-12}	2.02×10^{-12}	4.04×10^{-09}	5.86×10^{-11}	4.35×10^{-11}
375	5.86×10^{-09}	5.36×10^{-12}	5.22×10^{-12}	3.44×10^{-09}	1.15×10^{-10}	7.65×10^{-11}
455	5.28×10^{-09}	1.12×10^{-11}	1.08×10^{-11}	3.09×10^{-09}	1.98×10^{-10}	1.18×10^{-10}
535	4.89×10^{-09}	2.03×10^{-11}	1.94×10^{-11}	2.85×10^{-09}	3.14×10^{-10}	1.67×10^{-10}
615	4.61×10^{-09}	3.34×10^{-11}	3.14×10^{-11}	2.67×10^{-09}	4.65×10^{-10}	2.23×10^{-10}
695	4.38×10^{-09}	5.09×10^{-11}	4.71×10^{-11}	2.53×10^{-09}	6.54×10^{-10}	2.82×10^{-10}
775	4.19×10^{-09}	7.32×10^{-11}	6.67×10^{-11}	2.41×10^{-09}	8.83×10^{-10}	3.45×10^{-10}
855	4.02×10^{-09}	1.01×10^{-10}	9.00×10^{-11}	2.32×10^{-09}	1.15×10^{-09}	4.10×10^{-10}
935	3.87×10^{-09}	1.33×10^{-10}	1.17×10^{-10}	2.24×10^{-09}	1.46×10^{-09}	4.75×10^{-10}
1,015	3.73×10^{-09}	1.70×10^{-10}	1.46×10^{-10}	2.18×10^{-09}	1.81×10^{-09}	5.41×10^{-10}
1,095	3.59×10^{-09}	2.11×10^{-10}	1.78×10^{-10}	2.12×10^{-09}	2.19×10^{-09}	6.06×10^{-10}

correcting the **TS2** relative energies with their QZVPP values. Since the **C1** intermediate is already correctly described with a 3-ζ basis set, we are confident that the entrance channel is also well described at this level of theory. This is very convenient because QZVPP frequency calculations are quite expensive and many of them must be performed along the DCP. On the other hand, and as shown in our previous study [5], the exit channel plays a minor role when the reaction products are well below the reactants. This is due to the fact that the rate constant for **TS3** [strictly speaking, the sum of states for **TS3**, see Eq. 1] is very large compared to those for **TS1** and **TS2**, thus making the global rate coefficient independent of the dissociation process. For Mg^+, however, products are clearly above both reactants and **TS2**, and the exit channel is then expected to play a more important role in this reaction. In this case, consideration of QZVPP values for products' relative energies seems more appropriate taking into account the differences mentioned above between the 3-ζ and 4-ζ basis sets. However, let us point out that in the case that both **TS2** and products are clearly endothermic with respect to reactants, the reaction is not expected to proceed beyond the **C1** intermediate, at least under the experimental conditions of Zhao et al. [2]. The most important process in this case is the entrance channel. For this reason, we have decided to compute the exit channel using again the TZVPP basis set.

Experimental rate coefficients for Ca^+, Sr^+, and Ba^+ reactions have been obtained at 295 K by Zhao et al. [2]: $k = (2.6 \pm 0.8) \times 10^{-10}$ cm^3 molecule^{-1} s^{-1}, $k = (1.4 \pm 0.4) \times 10^{-11}$ cm^3 molecule^{-1} s^{-1}, and $k = (6.4 \pm 1.9) \times 10^{-11}$ cm^3 molecule^{-1} s^{-1}, respectively. Our theoretical predictions (4.99×10^{-10} cm^3 molecule^{-1} s^{-1}, 2.02×10^{-12} cm^3 molecule^{-1} s^{-1}, and 4.35×10^{-11} cm^3 molecule^{-1} s^{-1} (see Table 3) are in reasonable agreement with the experimental values. Let us point out that the predicted global rate constant for the Ca reaction shown in Table 3 differs with respect to that discussed in our previous work [5] in that we have used here a **TS2** relative energy (with respect to reactants) of −3.0 kcal/mol as obtained with the QZVPP basis set, somewhat larger than the relative energy used in [5], obtained with the TZVPP basis (−1.1 kcal/mol)[1]. In the case of Mg^+, for which no experimental results are available, we predict a very low rate coefficient (1.02×10^{-18} cm^3 molecule^{-1} s^{-1}). This is mainly due to the endothermicity of this reaction, as commented above. For the three reactions whose experimental rate constants have been measured, the errors on the computed ones are equivalent to kinetic barrier height misestimates of 0.9 kcal/mol (Ca^+), 1.1 kcal/mol (Sr^+), and 0.8 kcal/mol (Ba^+). It is important to stress at this point that bearing in mind the accuracy achieved by the levels of theory computationally affordable at present days to deal with the systems involved in the studied processes [35–37], the degree of agreement between the theoretically predicted rate constants and the corresponding experimental values can be considered acceptable (see for a detailed discussion on this subject Refs. [5, 38]).

As mentioned in the introduction and discussed in our previous article [5], an important goal of these studies is to assess the role played by the "outer" transition states (entrance channel) in controlling the kinetics of these reactions. Figure 2 shows the Arrhenius plots for the global rate constant, k_{global}, as well as its main components, k_{outer} and k_{inner}. In the case of Mg^+, we also collect the values of the rate constant for the exit channel (k_{exit}). These components describe the limiting behavior of the global rate constant when the dominant bottleneck for the reaction is provided by either the "outer" transition state, the "inner" transition state, or, in the case of Mg^+, the exit channel. The numerical rate constants for these limiting cases are also collected in Table 3.

For $Mg^+ + CH_3F$, a reaction that proceeds with a net activation barrier, we observe the expected Arrhenius plot (see Fig. 2). At low temperatures, k_{exit} clearly makes the largest contribution to k_{global} for this reaction. As temperature grows up, k_{exit} increases faster than k_{inner}, which becomes the dominant bottleneck for the reaction at high temperatures. As expected, k_{outer} does not appreciably contribute to the rate constant.

Zhao et al. [5] do not provide results for the reaction of Mg^+ with methyl fluoride, but similar experimental studies [6–8] with hydrocarbons and small inorganic ligands show that Mg^+ reactions proceed, if at all, by molecular addition. On the other hand, detection of Mg^+–CH_3F 1:1 clusters in helium buffer gas [9–11] by mass spectrometry suggests that this complex is stable enough toward dissociation. It is also interesting that in the experiments of Furuya et al. [9, 10] and Yang et al. [11], a small proportion of MgF^+ is also detected showing that, at least under their experimental conditions, Mg^+ is also able to activate C–F in methyl fluoride. In the experiments of Zhao et al. [2], addition is expected to occur in a termolecular fashion with helium atoms acting as the third body. In order to get more insights into the product distribution for this reaction, a pressure-dependent study should be done. This is beyond the scope of the present study, although work is in progress to address this point. On the other hand, experimental pressure-dependent studies are not available to the best of our knowledge either.

Arrhenius plots for the Ca^+ reaction are depicted in Fig. 2 and show that the global rate constant is mainly controlled by the inner bottleneck although with non-negligible contributions from k_{outer} particularly at very low temperatures. For a more detailed analysis of this reaction, we refer the reader to our previous study [5]. As expected, the reaction for Sr^+ and Ba^+ shows a qualitatively similar

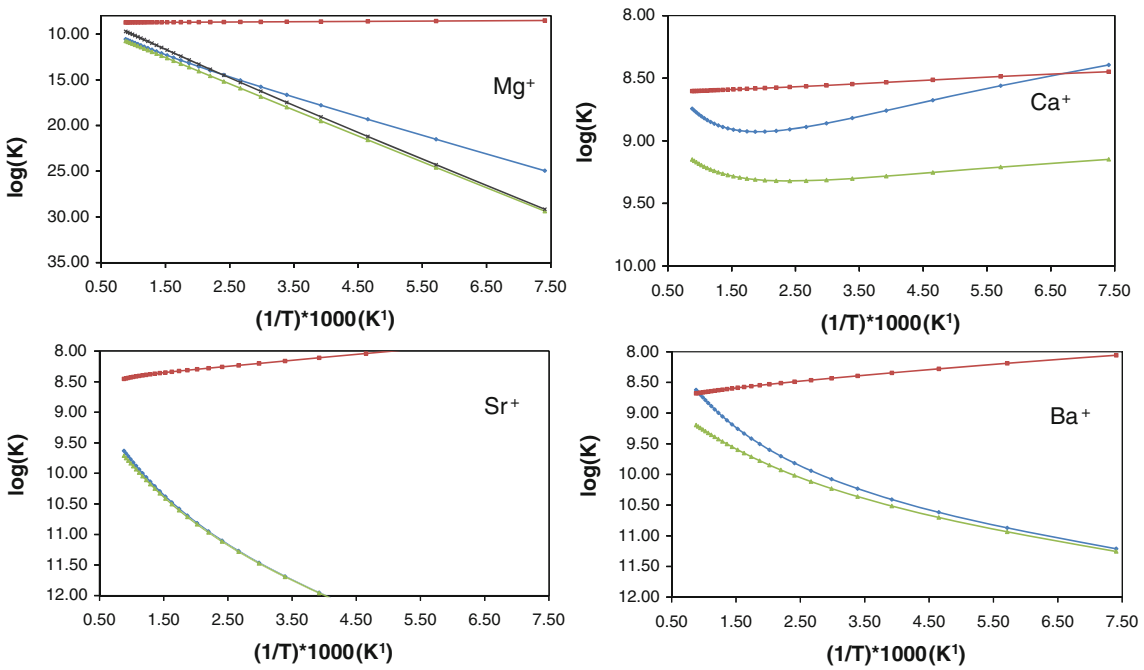

Fig. 2 Arrhenius plots (k given in cm^3 $molecule^{-1}$ s^{-1} and T in K) for the global rate constant, k_{global} (*green*), and its main limiting components (see the text for definitions): k_{inner} (*blue*), and k_{outer} (*red*) and k_{exit} (*gray*; only for Mg^+)

Table 4 MPW1K/TZVPP alkaline-earth metal, fluorine (parentheses), and CH_3 [brackets] partial charges (au) and spin densities according to Mulliken population analysis (MPA). MPA values for CH_3F are −0.312 (F) and 0.112 (C)

	Mg^+	Ca^+	Sr^+	Ba^+
Partial charge				
C1	0.885(−0.290)[0.405]	0.936(−0.352)[0.416]	0.954(−0.367)[0.413]	0.957(−0.370)[0.412]
TS2	1.095(−0.484)[0.388]	1.216(−0.591)[0.374]	1.272(−0.621)[0.349]	1.233(−0.580)[0.347]
C2	1.239(−0.534)[0.295]	1.502(−0.604)[0.102]	1.567(−0.651)[0.084]	1.599(−0.637)[0.038]
Spin density				
C1	0.993(−0.012)[0.020]	1.002(−0.008)[0.006]	1.002(−0.006)[0.004]	1.002(−0.002)[0.000]
TS2	0.528(0.004)[0.471]	0.579(−0.045)[0.468]	0.561(−0.039)[0.478]	0.615(−0.036)[0.420]
C2	0.187(0.012)[0.801]	0.076(−0.001)[0.925]	0.071(−0.001)[0.930]	0.039(0.000)[0.960]

behavior, but in these cases, the dominant contribution to k_{global} is definitely k_{inner}, except at very high temperatures. This is reasonable since the energy of **TS2** is higher for Sr^+ and Ba^+ than for Ca^+ (1.3, 0.4, and −3.0 kcal/mol, respectively).

Let us now briefly comment on the possible mechanisms for these reactions. Two plausible pathways have been proposed to interpret the experimental results available for these processes, namely single-electron transfer (SET, 'harpoon-like' mechanism) and oxidative addition (addition/elimination mechanism) [2, 4]. As suggested by Harvey et al. [4], the later mechanism is unlikely for alkaline-earth metal monocations because with only one unpair electron, they will not easily undergo insertion. The 'harpoon-like' mechanism, on the other hand, is supposed to take place through transfer of one electron from the metal monocation to methyl fluoride in the encounter adduct [3, 4]. We have collected in Table 4 the partial charges and spin densities for the three chemical fragments involved in these reactions (M^+, F, CH_3) as obtained with the Mulliken population analysis (MPA).

Data collected in Table 4 show that for the four monocations, the positive charge on the metal notably increases when passing from **C1** to **C2** through **TS2**, with a parallel increase in the negative net charge on the fluorine atom. The methyl group progresses toward the formation of a radical species (CH_3) at the same time. The spin density, initially (**C1**) mainly concentrated on the metal

monocation, is finally mostly located on the methyl group. Summarizing, data collected in Table 4 are fully compatible with the "harpoon-like" mechanism:

$$\begin{aligned} M^{\cdot+} + F - CH_3(\mathbf{R}) &\rightarrow M^{\cdot+} \cdots F - CH_3(\mathbf{C1}) \rightarrow \mathbf{TS2} \\ &\rightarrow M^{2+} \cdots F^{-} \cdots CH_3^{\cdot}(\mathbf{C2}) \\ &\rightarrow MF^{+} + CH_3^{\cdot}(\mathbf{P}) \end{aligned} \quad (2)$$

It has been suggested [3, 4] that if such a mechanism was in fact operating, an inverse correlation between the efficiency of the reaction and the SIE of the metal atom should be observed. The larger the SIE the higher the energy barrier associated with transition structure **TS2**. Thus, one would expect that the values of the SIEs should determine the relative magnitudes of the rate constants for the different cation metals. In the present case where SIE (Mg; 349 kcal/mol; MPW1K/QZVPP) $\gg$ SIE (Ca; 272 kcal/mol) $>$ SIE (Sr; 253 kcal/mol) $>$ SIE (Ba; 227 kcal/mol)[3] [39], the following condition $k(Mg^+) \ll k(Ca^+) \leq k(Sr^+) \leq k(Ba^+)$ should be expected. However, our kinetics calculations (see Table 3) predict $k(Mg^+) \ll k(Sr^+) < k(Ba^+) < k(Ca^+)$, in full agreement with the experimental observations that the reaction does not progress (or do it rather slowly) in the case of Mg^+ [6–11], and $k(Sr^+) = (1.4 \pm 0.4) \times 10^{-11}$ cm^3 molecule^{-1} s^{-1}, $k(Ba^+) = (6.4 \pm 1.9) \times 10^{-11}$ cm^3 molecule^{-1} s^{-1} and $k(Ca^+) = (2.6 \pm 0.8) \times 10^{-10}$ cm^3 molecule^{-1} s^{-1} [2].

Strictly speaking, the SIE values should correlate with the energy difference between **C1** and **TS2** (**C1** $\rightarrow$ **TS2** is basically a charge transfer process), provided charge transfer was the only force acting between the virtual fragments CH_3 and MF when reactants approach each other. However, while the (QZVPP) **C1** $\rightarrow$ **TS2** computed energy barriers are (see Table 2) 34.7, 19.8, 20.4, and 18.9 kcal/mol for Mg^+, Ca^+, Sr^+, and Ba^+ reactions, respectively, the corresponding SIE values are 347, 274, 255, and 230 kcal/mol. This plainly demonstrates that although charge transfer should be dominant, other contributions (electrostatic, dispersion, and/or induction contributions other than charge transfer) must play a role (responsible for the 0.6 kcal/mol energy difference between Ca^+ and Sr^+ reactions). Characterization of the different contributions is by no means a trivial task. Work in progress in that direction is under way in our laboratory.

On the other hand, we have pointed out in our previous work [5] that no correlation between the reaction global rate constants and the SIE should be expected if the kinetics of the reaction has non-negligible contributions from the outer transition state (see also [40, 41]). Such a correlation should only operate, if at all, for the rate constant associated with the **C1** $\rightarrow$ **TS2** process, not for the global rate constant. As commented above, we have shown in this study that for these reactions, even this correlation is, indeed, not as straightforward as expected.

[3] We would like to point out that the MPW1K/QZVPP SIE values are in very good agreement with the experimental ones: 347 kcal/mol (Mg), 274 (Ca), 254 (Sr), 231 (Ba).

4 Conclusions

A theoretical kinetics study by means of energy and total angular momentum resolved microcanonical variational/conventional theory has been carried out for the reactions between alkaline-earth metal monocations (Mg^+, Ca^+, Sr^+, and Ba^+) and methyl fluoride. The computed rate coefficients for the reactions of Ca^+, Sr^+, and Ba^+: 4.99×10^{-10} cm^3 molecule^{-1} s^{-1}, 2.02×10^{-12} cm^3 molecule^{-1} s^{-1}, and 4.35×10^{-11} cm^3 molecule^{-1} s^{-1} are in reasonable good agreement with the experimental values at 295 K: $k = (2.6 \pm 0.8) \times 10^{-10}$ cm^3 molecule^{-1} s^{-1}, $k = (1.4 \pm 0.4) \times 10^{-11}$ cm^3 molecule^{-1} s^{-1}, and $k = (6.4 \pm 1.9) \times 10^{-11}$ cm^3 molecule^{-1} s^{-1}, respectively. The theoretically predicted rate constant for the reaction of Mg^+ is very small (1.02×10^{-18} cm^3 molecule^{-1} s^{-1}), which is consistent with the experimental data available. The larger rate constant found for the calcium reaction is related to the low potential energy barrier at **TS2** (−3.0 kcal/mol) compared to Mg (+9.0), Sr (+1.3), and Ba (+0.4).

As a general conclusion, the studied reactions seem to proceed through a "harpoon-like" mechanism. We also notice the relative importance of other channels, apart from the "inner" bottleneck, to control the kinetics of these reactions. In the case of the Ca^+ reaction, where the formation of $CaF^+ + CH_3$ is an exothermic process, the "outer" bottleneck appreciably contributes to the global rate constant. For the Mg^+ reaction, contribution from the exit channel is not negligible as a consequence of the endothermicity of the formation of $MgF^+ + CH_3$. The reactions of Sr^+ and Ba^+ represent an intermediate situation: a low barrier at the "inner" bottleneck and the formation of products (SrF^+, BaF^+) being rather exothermic processes. Consequently, the reaction is fully controlled by the "inner" transition state.

Further work involving other metal cations, in progress in our laboratories, is required in order to confirm the general validity of the mechanistic findings reported in the present work.

Acknowledgments This research has been supported by the Ministerio de Educación y Ciencia of Spain (Grant CTQ2007-67234-C02), FICYT (Principado de Asturias, Spain; Grant IB08-23) and by the Junta de Castilla y León (Spain; Grant VA040A09). This work is dedicated to the memory of our colleague and friend Dr. Miguel Álvarez Blanco.

References

1. Mazurek U, Schwarz H (2003) Chem Commun 1321–1326
2. Zhao X, Koyanagi GK, Bohme DK (2006) J Phys Chem A 110:10607
3. Cornehl HH, Hornung H, Schwarz H (1996) J Am Chem Soc 118:9960
4. Harvey JN, Schröder D, Koch W, Danovich D, Shaik S, Schwarz H (1997) Chem Phys Lett 278:391
5. Varela-Álvarez A, Rayón VM, Redondo P, Barrientos C, Sordo JA (2009) J Chem Phys 131:144309
6. Milburn RK, Hopkinson AC, Bohme DK (2000) J Phys Chem A 104:3926
7. Milburn RK, Baranov V, Hopkinson AC, Bohme DK (1998) J Phys Chem A 102:9803
8. Milburn RK, Baranov V, Hopkinson AC, Bohme DK (1999) J Phys Chem A 103:6373
9. Furuya A, Misaizu F, Ohno K (2006) J Chem Phys 125:094309
10. Furuya A, Misaizu F, Ohno K (2006) J Chem Phys 125:094310
11. Yang X, Hu Y, Yang S (2000) J Phys Chem A 104:8496–8504
12. Lynch BJ, Fast PL, Harris M, Truhlar DG (2000) J Phys Chem A 104:4811
13. Weigend F, Ahlrichs R (2005) Phys Chem Chem Phys 7:3297
14. Dunning TH (1989) J Chem Phys 90:1007
15. Koput J, Peterson KA (2002) J Phys Chem A 106:9595
16. Prascher BP, Woon DE, Peterson KA, Dunning TH Jr, Wilson AK (2010) Theor Chem Acc. doi:10.1007/s00214-010-0764-0
17. Jensen F (2001) J Chem Phys 115:9113
18. Jensen F (2007) J Phys Chem A 111:11198
19. Feller D (1996) J Comp Chem 17:1571
20. Schuchardt KL, Didier BT, Elsethagen T, Sun L, Gurumoorthi V, Chase J, Li J, Windus TL (2007) J Chem Inf Model 47:1045
21. González C, Schelegel HB (1989) J Chem Phys 90:2154
22. González C, Schelegel HB (1990) J Phys Chem 94:5523
23. McQuarrie DA (1973) Statistical thermodynamics. University Science Books, Mill Valley
24. Frish MJ, Trucks GW, Schlegel HB et al (2004) GAUSSIAN 03, C.01. Gaussian Inc., Wallingford
25. Mozurkowich M, Benson SW (1984) J Phys Chem 88:6429
26. Garret BC, Truhlar DG (1979) J Chem Phys 70:1593
27. Hu X, Hase WL (1991) J Chem Phys 95:8073
28. Villá J, Truhlar DG (1997) Theor Chem Act 97:317
29. Villá J, González-Lafont A, Lluch JM, Corchado JC, García-Espinosa J (1997) J Chem Phys 107:7266
30. Forst W (1973) Theory of unimolecular reactions. Academic, New York
31. Lias SG, Bartmess JE, Liebman JF, Holmes JL, Levin DR, Mallard WG (1988) J Phys Chem Ref Data 17(Suppl 1):1
32. Chase MW, Davies CA, Downey JR, Fruip KJ, McDonald RA, Syverud AN (1985) J Phys Chem Ref Data 14 (Suppl 1)
33. Partridge H, Langhoff SR, Bauschlicher CW Jr (1986) J Chem Phys 84:4489
34. Boese AD, Martin JML, Handy NC (2003) J Chem Phys 119:3005
35. Feller D, Sordo JA (2000) J Chem Phys 112:5604
36. Feller D, Sordo JA (2000) J Chem Phys 113:485
37. Sordo JA (2001) J Chem Phys 114:1974
38. Varela-Álvarez A, Markovic D, Vogel P, Sordo JA (2009) J Am Chem Soc 131:9547
39. Bashkin S, Stoner Jr. JO (1975) Atomic energy levels and Grotrian diagrams. North-Holland publishing company, New York
40. Greenwals EE, North SW, Georgievskii Y, Klippenstein SJ (2005) J Phys Chem A 109:6031
41. González-Lafont A, Lluch JM (2004) J Mol Struct (THEOCHEM) 709:35